Chapter 8
Carbon-Based Nanomaterials for Carbon Dioxide Reduction Reaction

Dongping Xue and Yifan Wei

Abstract Electrochemical reduction of CO_2 with renewable electricity has attracted much attention for producing fuels and value-added chemicals while reducing carbon emissions. Carbon-based nanomaterials are of particular interest due to their earth abundance and low cost. In this chapter, the latest progress and research status of four types of nanomaterials in electrocatalytic carbon dioxide reduction reaction (CO_2RR) have been discussed in detail, including metal-free carbon-based, atomically dispersed carbon-based, metal nanoparticles encapsulated carbon-based, and metal nanoparticles supported carbon-based nanomaterials. Finally, the challenges and opportunities faced by carbon-based nanomaterials in electrochemical CO_2RR have been proposed, as well as possible solutions in the future.

8.1 Introduction

Due to the continuous growth of human society's demand for energy, the consumption of non-renewable fossil fuels has increased dramatically, releasing a large amount of greenhouse gas carbon dioxide (CO_2). As of 2020, the concentration of CO_2 in the atmosphere has exceeded 414 ppm and continues to increase, causing environmental problems such as global warming and ocean acidification, which have attracted widespread attention [1]. In addition, there is an urgent need to explore technologies that can address both carbon emissions and the energy crisis, guided by the national strategy of "emission peak and carbon neutrality". In the past few decades, various technologies such as biochemical, electronic, photochemical, radiochemical, and thermochemical have been developed to reduce CO_2 [2–5]. Among them, electrocatalytic CO_2RR technology, with its simple experimental equipment, mild reaction conditions, and the use of renewable energy to provide electricity, is

D. Xue (✉) · Y. Wei
College of Materials Science and Engineering, Zhengzhou University, Zhengzhou 450001, P. R. China
e-mail: xdongping1231@126.com

Y. Wei
e-mail: Ivan98cn@163.com

J.-N. Zhang (ed.), *Carbon-Based Nanomaterials for Energy Conversion and Storage*,
Springer Series in Materials Science 325, https://doi.org/10.1007/978-981-19-4625-7_8

an effective way to achieve relatively "zero-emission" of CO_2 and store renewable energy [6–8]. In addition, electrocatalytic CO_2RR technology can utilize solar energy, wind energy, tidal energy, and other renewable energy sources to effectively reduce CO_2 into important fuels and chemical raw materials, such as formate/formic acid ($HCOO^-$/HCOOH), carbon monoxide (CO), methane (CH_4), methanol (CH_3OH), ethylene (C_2H_4), and ethanol (C_2H_5OH). Such chemicals will be needed for a long time in the future, however, the current preparation methods are not only dominated by carbon-intensive fossil fuel methods, but also under harsh preparation conditions (Fig. 8.1) [9]. Therefore, utilizing electrocatalytic CO_2RR technology to make carbon chemicals may be a more sustainable alternative to this difficult-to-decarbonize approach.

Linear CO_2 molecules are relatively thermodynamically stable and chemically inert, reducing the kinetics of the reduction reaction, while the electrocatalytic reduction conversion efficiency is closely related to the slow kinetics of the rate-determining step [10]. Moreover, the selectivity of these catalysts remains low due to complicated reaction mechanisms [11]. In this regard, developing durable and highly efficient electrocatalysts is of vital importance to accelerate the reaction kinetics and thus improve the overall energy conversion efficiency. At present, the selection of electrocatalysts is mainly focused on precious metals such as Pt and Au [12]. However, the high cost, poor long-term stability, and low natural reserves of noble metal electrocatalysts hinder their commercialization. Carbon-based nanomaterials have become one of the main effective materials to replace noble metal catalysts due to the advantages of wide source of raw materials, controllable structure, good chemical stability, and electrical conductivity [13, 14]. Despite these advantages,

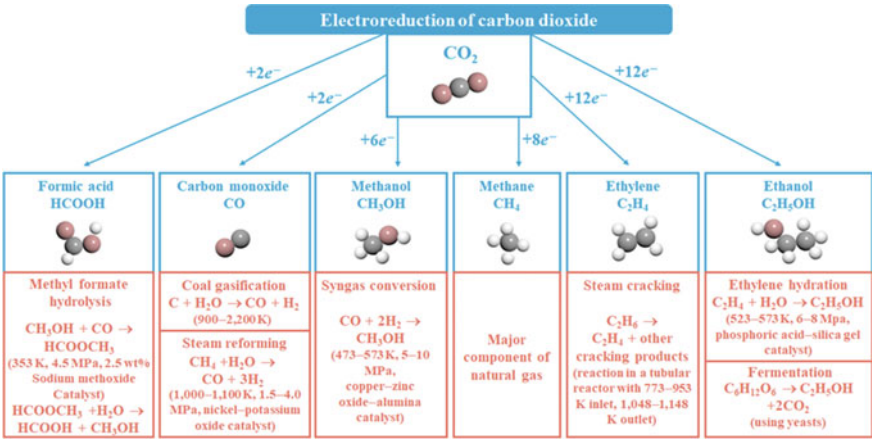

Fig. 8.1 Overview of select CO_2 electroreduction products, along with the current industrial methods to manufacture these products. The current large-scale methods to manufacture HCOOH, CO, CH_3OH, CH_4, C_2H_4, and C_2H_5OH are primarily fossil fuel based and, in most scenarios, require high pressure and/or high temperature to drive the process. The electroreduction of CO_2 could be an alternative sustainable pathway to such fossil fuel-based manufacturing methods

there is still a large gap between the electrocatalytic performance of pure carbon nanomaterials and precious metals.

After Dai's pioneering work on nitrogen-doped carbon nanotubes was published in 2009, high-performance CBN containing various defects have attracted the interest of many researchers [15]. The introduction of defects can affect the overall charge state of the carbon skeleton, thereby increasing the density and activity of potential active sites and improving the overall electrocatalytic performance of carbon nanomaterials [16, 17]. For example, edge and topological defects have been studied extensively in electrocatalytic reactions such as HER and oxygen reduction reaction (ORR) because of their different electrochemical and thermodynamic properties from the matrix material [18, 19]. Their potential for electrocatalytic CO_2 reduction has only recently been recognized. In addition, the doping of heteroatoms (N, B, P, etc.) [20] and the introduction of single metal atoms (Ni, Mn, and Cu, etc.) [21–23] can also effectively improve the performance of electrocatalytic CO_2 reduction. However, a major problem of nonprecious metal catalysts is their poor stability in practical catalytic processes, especially in harsh environments (e.g., strong acidity or alkalinity, high temperature, and high overpotential). Recently, to overcome the low stability of nonprecious metal catalysts under harsh reaction conditions, Bao et al. designed and fabricated unique chainmail catalysts by fully encapsulating transition metals through graphene shells. which can effectively improve the activity and stability of nonprecious-metal catalysts [24, 25]. Strong metal-support interaction (SMSI), commonly happening between metal and metal oxide support, has drawn significant attention in heterogeneous catalysis due to its capability of enhancing the activity and stability of catalysts. Herein, the strong interaction between metal oxide and carbon supports is discovered to significantly boost the performance for electrocatalytic CO_2 reduction reaction (CO_2RR) [26].

In this chapter, a systematic overview of the latest developments and structure-effect relationships in the electrocatalytic reduction of CO_2 from four classes of materials (metal-free carbon-based electrocatalysts, atomically dispersed metal carbon-based electrocatalysts, metal nanoparticles encapsulated/supported carbon-based electrocatalysts) have been presented. It is hoped that this chapter will provide a reference for researchers interested in CO_2 electrocatalytic reduction, to solve the technical bottlenecks from the aspect of catalytic materials and realize the industrialization of CO_2 electrocatalytic reduction in the near future.

Before conducting a detailed summary analysis of a certain class of materials, the commonly used evaluation parameters for electrocatalytic CO_2RR for the convenience of readers have been briefly summarized. The key performance parameters used to evaluate the activity, selectivity, and stability of electrocatalysts for CO_2RR are mainly overpotential, Faraday efficiency, Tafel slope, and energy efficiency.

(1) Overpotential. Overpotential is the difference between working potential and theoretical potential, which reflects the driving force of ECR.
(2) Energetic efficiency (EE). EE represents the overall energy utilization rate forming the target product.

(3) Faradaic Efficiency (FE). FE represents the percentage of the charge consumed by the reaction to form the target product over the total charge transferred during the reaction. It can be calculated by Eq. (8.1):

$$\mathrm{FE} = \frac{\alpha n F}{Q} \tag{8.1}$$

where α is the number of electrons transferred per molecule of the target product (e.g., α = 2 for reduction of CO_2 to CO), n is the number of moles of the target product make by the reaction, F is the Faraday constant (96485 C mol^{-1}), and Q represents the charge passed during the entire reaction. The FE directly reflects the selectivity of the catalyst for ECR.

(4) Tafel slope. The Tafel slope indicates the relationship between the overpotential and the logarithm of the current density, where the current density is obtained by dividing the total current by the geometric surface area of the working electrode. It is generally believed that the smaller the Tafel slope, the better the catalytic performance of the electrocatalyst.

8.2 Metal-Free Carbon-Based Electrocatalysts for CO_2RR

With the deepening of research, it has been found that the catalytic activity of undoped carbon nanomaterials can also be greatly improved by rationally regulating the intrinsic carbon defects within the carbon framework. Intrinsic carbon defects are formed by thermal vibrations of lattice atoms in the absence of any dopants, mainly including edges, vacancies, holes or topological defects [14, 27]. Among them, the intrinsic carbon defects used in ECR are mainly edge and topological defects. The main effects on the electrocatalytic CO_2RR catalysts are as follow: (1) Edge defects, which make the material edge full of a large number of unpaired π electrons, can effectively accelerate the transfer of electrons and reduce the formation energy of key intermediates. At the same time, the edge carbon atoms show higher charge density and can be used as active sites [27]. (2) Topological defects, the introduction of topological defects will interfere with the electronic symmetry of aromatic rings, causing local charge redistribution, and the adjacent carbon atoms can be optimized to become the active sites of the electrocatalyst [28–30]. Exploring the preparation of defective sites with suitable CO_2 activation/adsorption energies is an effective way to design high-performance CO_2RR catalysts. Thus, Wu et al. [31] prepared a defect-rich hierarchical porous carbon catalyst (DHPC) by pyrolysis of ZnO NP@ZIF-8 with the help of KNO_3 and ZnO nanoparticles (ZnO NPs), which acted as oxygen suppliers and carbon modifiers to facilitate carbon deficient site/Lewis base site generation (Fig. 8.2a, b). The mesoporous and carbon defect structure in DHPC improved its adsorption and activation efficiently for CO_2. FE_{CO} can reach 99.5% at −0.5 V versus reversible hydrogen electrode (*vs.* RHE) in 0.5 M $KHCO_3$ medium. More importantly, such carbon material is useful even in a real

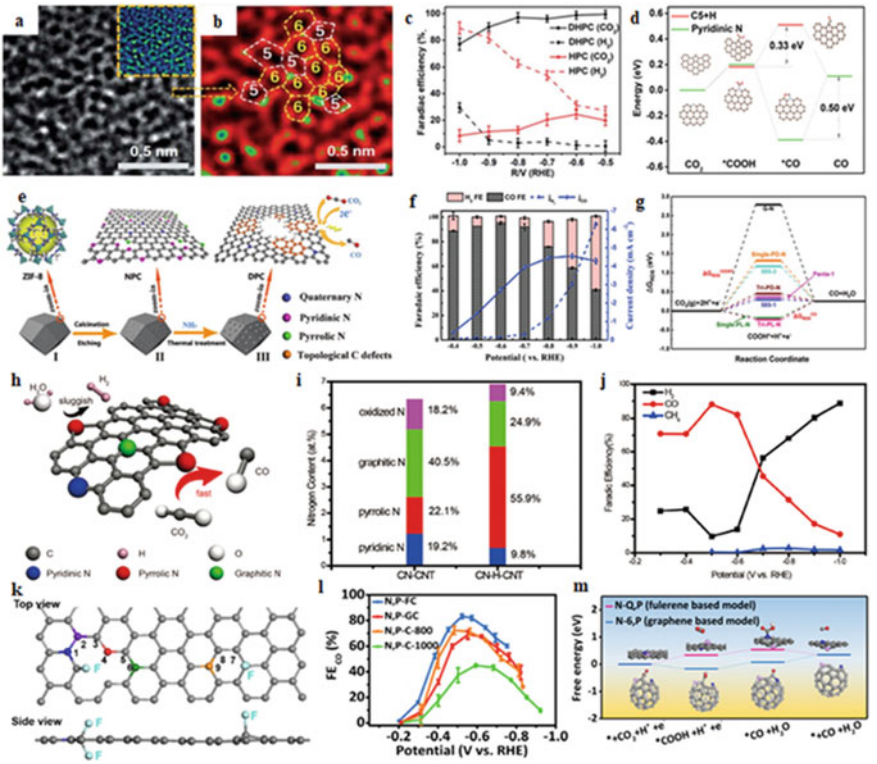

Fig. 8.2 Metal-free carbon-based electrocatalysts. Magnification of one segment of the HRTEM image **a** and **b** after fast Fourier transformation (FFT) filtering. **c** Faradaic efficiencies of DHPC and HPC in 0.5 M $KHCO_3$ at various potentials. **d** Free energy diagram for CO_2 reduction to CO over different defect sites. Reproduced with permission [31]. [32][43][45][46] Copyright 2020, Royal Society of Chemistry. **e** CO_2 electrochemical reduction capability of CN-H-CNTs and passivation for HER reaction. Summary of N atomic contents and total atomic concentrations in **f** CN-CNTs. Faradaic efficiency for CO, H_2, and CH_4 versus potential on **g** CN-H-CNTs. Reproduced with permission. Copyright 2019, John Wiley and Sons. **h** Top view and side view of DFT model for FC. Gray atom: carbon, light blue atom: fluorine, other colorful atoms: carbon that calculated as active sites. **i** The FE_{CO} for various catalysts. **j** Free energy diagram of ECR reaction to CO on various catalysts. Reproduced with permission. Copyright 2017, John Wiley and Sons. **k** Top view and side view of DFT model for FC. Reproduced with permission. Copyright 2018, John Wiley and Sons. **l** FE for CO production at different applied potentials. **m** Free energy pathway of CO_2RR on N-Q,P and N-6,P. Reproduced with permission. Copyright 2019, Royal Society of Chemistry

sea-water medium with high CO faradaic efficiency as well (96.5% at −0.6 V) (Fig. 8.2c). According to the characterization test and theoretical calculation results, pentagon defects are proved to be electrocatalytic active centers, which can lead to local electron density redistribution, and have stronger adsorption on reactants and intermediates (Fig. 8.2d). Zhang et al. [32] reported a positive correlation between the electrocatalytic CO_2RR performance of carbon-based catalysts and the content

of intrinsic carbon defects within the catalysts. They synthesized a series of defective N-doped carbon spheres, it is demonstrated that the defective porous carbon catalyst without active heteroatom doping also exhibits good catalytic performance for electrocatalytic CO_2RR (Fig. 8.2e, f). The NEXAFS spectra show that the defects of sp^2 (octagonal and pentagonal) rather than the edges of sp^3 (armchair and zigzag) are positively related to the ECR activity of the defective porous carbon catalysts, and as the pyrolysis temperature increases, the more defects, the better the activity and selectivity of the catalyst. This conclusion is also verified by DFT calculation, for perfect sp^2 carbons, the free energies required for the formation of COOH* for armchair and zigzag edge defects increase significantly, while the free energy required for pentagonal defects decreases significantly (Fig. 8.2g). For the octagonal defect, due to the optimization of COOH* adsorption, part of the positive C atoms facilitates the conduction of electrons, which further promotes the reduction of COOH* to CO*. Although defect-based carbon materials exhibit a great potential in the diversity of electrocatalyst structural design. However, due to the difficulty of introducing a large number of specific types of defects, the structure-performance relationship between defective carbons and CO_2RR electrocatalysis has not been fully established.

Besides intrinsic defective carbon-based catalysts, heteroatom-doped carbon-based catalysts are another very important class of metal-free carbon-based electrocatalysts. Heteroatom doping with different electronegativity into the carbon network will introduce asymmetric charge, redistribute the spin density, break the electrical neutrality of carbon matrix, optimize the electronic properties of carbon materials to induce the generation of charged active sites [29, 33, 34]. In addition, the doping of heteroatoms can also stimulate the adjacent carbon atoms to improve the conductivity of carbon materials, thus enhancing the overall electrocatalytic activity of carbon materials [35]. The heteroatoms incorporated into carbon-based materials to enhance catalytic performance are generally B, [36] N, [37] O, [38] F, [39] P, [40] and S [41]. Among them, N atom is the most commonly used doped heteroatom because of its smaller atomic radius and larger electronegativity than carbon atom. N-doping in carbon nanomaterials generally forms four kinds of N-containing configurations including pyridinic, pyrrolic, graphitic, and oxidized N [42]. Most studies consider pyridinic-N as the primary active site for CO_2RR among the four N-containing configurations although different views are present. It is proposed that pyridinic-N can significantly enhance the binding of CO_2 or key intermediates as compared to graphitic-N or pyrrolic-N because of its accessible lone pair electrons. Zheng et al. [43] developed a unique vapor-etching method for tuning the configuration of nitrogen dopants in carbon frameworks. Selective etching takes advantage of the fact that H_2O molecules prefer to bond with carbon atoms around graphitic-N and pyridinic-N. After vapor etching, pyrrolic-N atoms with low water affinity are retained as the dominant N type in the obtained N-doped carbon network (designed as CN-H-CNT) (Fig. 8.2h) with a much increased content from 22.1 to 55.9 at % among the total N species (Fig. 8.2i). This steam-etched CN-H-CNT catalyst enables an excellent CO_2 reduction catalytic activity and HER suppression, with a high CO_2RR selectivity (~88%) toward the formation of CO under −0.5 V versus RHE. (Fig. 8.2j). The above work provides a new strategy for tuning the intrinsic

configuration of N-doped carbon and developing efficient and stable carbon cycle catalysts. On the other hand, doping F into the carbon lattice is different from N doping (replacement of carbon atoms in the lattice), which forms C-F bonds with covalent, ionic or semi-ionic properties [44]. Since F has the greatest electronegativity, the bonded carbon atoms will have more positive charges and become the active sites for electrocatalytic CO_2RR, which will be more favorable for the electrocatalytic CO_2RR [39]. Xie et al. [45] synthesized a F-doped carbon (FC) catalyst by simply pyrolyzing a mixture of commercial BP 2000 and polytetrafluoroethylene (PTFE) as a fluorine source (Fig. 8.2k). The FE of this catalyst electrocatalytic CO_2RR to CO reaches a maximum value (90%) at a lower overpotential (-0.51 V *vs.* RHE). Both experiments DFT calculations demonstrate that the key role of F doping in promoting the reduction of CO_2 to CO on metal-free carbon catalysts should have three functions: (1) Introduce a positive charge density between adjacent defect carbon atoms; (2) Introduce asymmetric spin density into adjacent defect carbon atoms; through these effects, carbon atoms become highly active and bind more strongly to COOH*, thereby increasing the reaction rate at lower overpotentials; (3) The Gibbs free energy of adsorbed H* is increased, resulting in the inhibition of the competitive hydrogen evolution reaction (HER) on the FC. In this regard, enhanced reduction of CO_2 to CO can be achieved over FC catalysts.

The diatomic co-doping may bring about the catalytic activity that the single heteroatom doped carbon material does not have because of the synergistic effect. Zhang et al. [46] prepared N,P-coordinated fullerene-like carbon (N,P-FC) and N,P-coordinated graphite-like carbon (N,P-FC) by soft-template pyrolysis method for electrocatalytic CO_2RR performance test. Different pyrolysis temperatures make the samples have different P/N atomic ratios, and the catalytic activity of the samples increases with the increase of the P/N atomic ratio. The N,P-FC obtained by pyrolysis at 900 °C has the best electrocatalytic CO_2RR activity (Fig. 8.2l). At the same time, it is found and confirmed by DFT that fullerene structure is more beneficial to electrocatalytic CO_2RR than graphene structure (Fig. 8.2m). Consequently, the above studies provide guidance and reference for designing and synthesizing high efficiency, high selectivity, and low cost heteroatom-doped carbon materials to replace metal catalysts for efficient electrocatalytic CO_2RR.

The co-doping of two different elements in carbon materials provides a new opportunity for the application of electrocatalysts. By properly adjusting the precursor, dopant type, doping ratio, and spatial distribution configuration, the electrocatalytic CO_2RR performance of the carbon-based catalyst is optimized.

8.3 Atomically Dispersed Metal Carbon-Based Electrocatalysts for CO_2RR

In recent years, atomically dispersed metal carbon-based nanomaterials have become popular and effective electrocatalysts for improving the performance of electrocatalytic CO_2RR due to their near 100% atomic utilization and excellent catalytic performance [47, 48]. Among them, the main reasons for the excellent electrocatalytic CO_2 reduction performance of metal-N–C catalysts are as follows. (1) Metal atoms directly combine with C-N atoms in carbon network to form metal activity centers with dispersed atoms [49]. (2) The size effect of single metal atoms gives carbon-based nanomaterials unique electronic structural characteristics and high specific surface area [50]. (3) The introduction of metal atoms changes the coordination environment of surface atoms, reduces the coordination number of surface atoms, decreases the overpotential of the catalyst, increases the current density of the catalyst, and reduces the Gibbs free energy of the formation of key intermediates and the desorption energy of the final product in ECR reaction [51]. M-N-C catalyst has been widely used in the study of ORR for decades, but were used to study electrocatalytic CO_2RR was for the first time proposed by Strasser et al. [52] in 2015 that Fe-N-C, Mn-N-C, and Fe, Mn-N-C have high electrocatalytic CO_2RR performance. The metals used to form M-N-C catalysts are mainly transition metals and individual precious metals such as Fe, Co, Ni, Cu, and Pd. Kattel et al. [53] prepared a N-doped carbon-supported Pd single-atom catalyst (Pd-NC) with Pd-N_4 sites. The well-dispersed Pd-N_4 active centers in the catalyst help stabilize the adsorbed CO_2 reduction intermediates, thereby enhancing the ECR ability at low overpotentials. However, due to the rarity and expensiveness of precious metals, low-cost transition single metal atom catalysts that can achieve the catalytic activity of precious metals are currently hot research topics. Wang et al. [54] successfully introduced a single P atom into an N-doped carbon-loaded single Fe atom catalyst (Fe-SAC/NPC), mainly in the form of a P–C bond for the electroreduction of CO_2 to CO in aqueous solution (Fig. 8.3a). Fe K-edge X-ray absorption spectroscopy (XAS) results indicate that the presence of P reduced the oxidation state of Fe in Fe-SAC/NPC. By fitting the FT-EXAFS spectra of Fe-SAC/NPC and Fe-SAC/NC in *R* space, the local structure of Fe was identified, in which each Fe atom was isolated by four N atoms and one O atom (Fig. 8.3b). This catalyst exhibited a CO Faradaic efficiency (FE_{CO}) of ~ 97% (Fig. 8.3c) and a stable CO partial current density (J_{CO} of ~ 5 mA cm^{-2} for at least 24 h at a low overpotential of 320 mV with a Tafel slope of only 59 mV dec^{-1}, exceeding most reported single-atom catalysts and comparable to the most advanced gold catalysts to date. By combining experiments and DFT calculations, it was demonstrated that the presence of a single P atom increases the electron density at the Fe center and COOH* formation is greatly facilitated, resulting in excellent CO_2RR performance at low overpotentials. Among currently identified materials, Cu is the only recognized material catalyzing the production of a large number of hydrocarbons or alcohols in aqueous solutions [55, 56]. He et al. [57] design a facile procedure to synthesize through the hole carbon nanofibers (TCNFs) with abundant and homogeneously

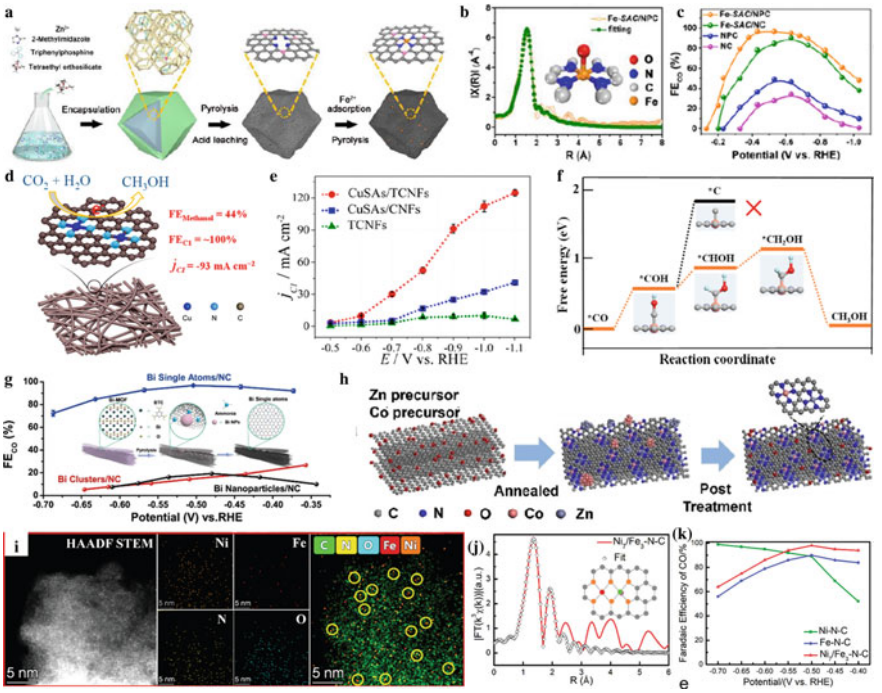

Fig. 8.3 Atomically dispersed metal carbon-based electrocatalysts. **a** Scheme of the synthesis of Fe-SAC/NPC. **b** *R* space fitting curve of Fe-SAC/NPC with the coordination model of Fe. **c** FE_{CO} of Fe-SAC/NPC. Reproduced with permission [54]. [57][58][60][61] Copyright 2021, John Wiley and Sons. **d** Synthesis procedure of CuSAs/THCF. **e** Partial current density of three samples. **f** Free energies for conversion of *CO to CH_3OH on Cu-N_4 structure. Reproduced with permission. Copyright 2019, American Chemical Society. **g** Scheme of the transformation from Bi-MOF to single Bi atoms. Reproduced with permission. Copyright 2019, American Chemical Society. **h** Schematic illustration of ZnCoNC synthesis. Reproduced with permission. Copyright 2020, John Wiley and Sons. **i** HAADF STEM image and representative EDS chemical composition of the Ni_7/Fe_3-N-C sample. **j** Ni_7/Fe_3-N-C samples (Ni, Fe, O, N, and C atoms are represented in red, green, pink, orange and grey, respectively.) **k** FE of CO at various potentials. Reproduced with permission. Copyright 2021, Royal Society of Chemistry

distributed Cu single atoms (CuSAs) for efficient electrochemical CO_2RR (Fig. 8.3d). Due to the excellent mechanical properties, CuSAs/TCNFs can be directly used as the cathode for CO_2RR. Due to the synergistic effect of the through-hole carbon structure and abundant isolated Cu active sites, the CuSAs/TCNFs exhibited a FE of 44% and a methanol partial current density of −93 mA cm^{-2} as well as long-term stability (Fig. 8.3e). DFT calculations from CO* to methanol were performed (Fig. 8.3f). According to DFT calculations, the reduction of COH* to CHOH* on the Cu-N_4 structure has a moderate free energy barrier (~0.86 eV). In contrast, COH* to C* exhibits a higher reaction free energy barrier (~1.88 eV), which is also higher than that of other reaction steps in the CH_3OH generation process. Therefore, the Cu single-atom sites on the CuSAs/TCNFs catalysts tend to generate CH_3OH rather

than CH_4. Besides transition metals, P-block metals are also widely used for electrocatalytic CO_2RR. For example, Li et al. [58] devised a simple and novel route to develop catalysts composed of single Bi atoms on N-doped carbon networks (Bi SAs/NCs) with hierarchical porosity for efficient CO reduction (Fig. 8.3g). Catalyst exhibits high intrinsic CO_2 reduction activity for CO conversion, with high FE_{CO} (97%) and large turnover frequency (5535 h^{-1}) at a low overpotential of 0.39 V versus RHE. Further experiments and DFT calculations reveal that the single-atom Bi-N_4 site is the main active center for CO_2 activation and rapid formation of the key intermediate COOH* with a low free energy barrier.

Researchers further found that the interactions between tight single atoms can have a dramatic impact on catalytic performance compared to isolated atoms, as they can optimize intermediate adsorption and thus product distribution [59]. Gong et al. [60] synthesized Zn/Co–N-C catalysts by pyrolysis and post-acid treatment (Fig. 8.3 h). Performance test results show that Zn/Co-N-C has a high FE_{CO} of 93.2% was achieved at −0.5 V versus RHE and a CO current density of about 26 $mAcm^{-2}$ at −0.5 V remained stable after a 30 h test. DFT calculations indicate that the electronic effect between Zn and Co lowers the energy barrier for the formation of COOH* on the Zn site, promoting the reduction of CO_2 to CO. Arbiol et al. [61] prepared a quasi-double star Ni/Fe-N-C catalyst consisting of nearby Ni and Fe active sites by simple pyrolysis of Ni and Fe co-doped Zn-based MOFs in order to achieve high selectivity at low overpotentials during the CO_2 reaction (Fig. 8.3i). The atomic structure of the Ni/Fe–N-C catalyst was verified in detail by EXAFS spectra (Fig. 8.3 j), and based on the fitting results and the corresponding fitting parameters, it was demonstrated that a single Fe atom should be coordinated to four N atoms and one O atom. Performance testing found that the optimized Ni/Fe-NC catalyst exhibited unique selectivity (98% maximum FE(CO)) at a low overpotential of 390 mV versus RHE, which was superior to its single metal counterpart (Ni-N-C and Fe-N-C catalysts) and other state-of-the-art M-N-C catalysts (Fig. 8.3k). DFT results further suggest that tuning catalytic CO_2RR performance through nearby Ni and Fe active sites may break the activity benchmark for single-metal counterparts, as adjacent Ni and Fe active sites not only act synergistically to reduce COOH* formation and CO* desorption reaction barriers, but also prevent the undesired hydrogen evolution reaction (HER) compared to their single metal counterparts.

By constructing suitable carbon precursor materials, individual metal atoms can be trapped and stabilized. Due to the large difference in electronegativity between metal and carbon atoms, sufficient charge transfer can be generated to make this structural unit (M-N-C/M-C) an active center for electrocatalysis, reducing the activation energy barrier and overpotential of the reaction. These strategies provide important guidance for the preparation of high-performance electrocatalytic CO_2RR catalysts and are also one of the current research hotspots.

8.4 Metal Nanoparticles Encapsulated/Supported Carbon-Based Electrocatalysts for CO_2RR

The best catalytic activity of atomically dispersed transition metal carbon-based catalysts is basically comparable to that of precious metals, but their poor stability seriously hinders their commercial application. Recently, to overcome the low stability of nonprecious metal catalysts, Bao et al. [24, 25] proposed a novel and promising strategy to design and fabricate unique chainmail catalysts by fully encapsulating transition metals through graphene shells. In this carbon layer encapsulated transition metal catalyst, the electron of transition metals can penetrate through the graphene shell to promote the catalytic reaction on the external graphene surface, while the graphene shell can completely prevent reaction molecules and medium from contacting the transition metals and therefore can protect the transition metals from damage in harsh conditions. It will improve both the activity and stability of nonprecious-metal catalysts [25]. For example, Ye et al. [62] prepared Fe@C hybrids by a two-step calcination method using MIL-101(Fe) as precursor (Fig. 8.4a). The activity and selectivity to CO for Fe@C, Fe/SiO_2, and Fe/CNT samples are summarized in Fig. 8.4b. Fe@C catalyst exhibits the highest catalytic activity toward the CO generation (55.75 $\mu mol\ min^{-1}$), the preferred selectivity toward CO over Fe@C catalyst (99.76%) become much obvious by evaluating in the fixed-bed reactor. DFT calculations were carried out to gain further insights into the nature of this catalytic process (Fig. 8.4c). Density of states (DOS) calculations show that the electronic structure of Fe nanoparticles near the Fermi energy level is modified to a metallic state by charge transfer and the Fermi energy level rises, thus ensuring the electron transfer of Fe nanoparticles to the reactants during catalysis and enhancing the catalytic performance.

Strong metal-support interaction (SMSI), commonly happening between metal and metal oxide support, has drawn significant attention in heterogeneous catalysis due to its capability of enhancing the activity and stability of catalysts. Herein, the strong interaction between metal and carbon supports is discovered to significantly boost the performance for electrocatalytic CO_2 reduction reaction (CO_2RR) [26]. He et al. [63] report the synthesis of copper clusters supported on defect-rich carbon (DRC) with an abundant microporous structure by a very simple synthetic route involving first impregnation at 800 °C and subsequent calcination at 600 °C. The dual confinement of carbon defects and microporosity effectively prevented metal aggregation during calcination, resulting in copper clusters with a diameter of ~1.0 nm and containing ~10 atoms (Fig. 8.4d). The resulting Cu clusters/DRC showed excellent performance in CO_2RR, with a high FE of 81.7% for CH_4 and a partial current density of 18.0 mA cm^{-2} at 1.0 V versus RHE (Fig. 8.4e), which exceeded most Cu-based electrocatalysts. This can be attributed to the sub-nanoscale Cu clusters, whose *d*-band centers are shifted upwards compared to the nanoparticles, which can enhance the adsorption strength of H* and CO*, thus promoting the formation of CH_4 (Fig. 8.4f). In addition, the SMSI effect of Cu clusters and defective carbon also contributes significantly to the excellent performance by tuning the

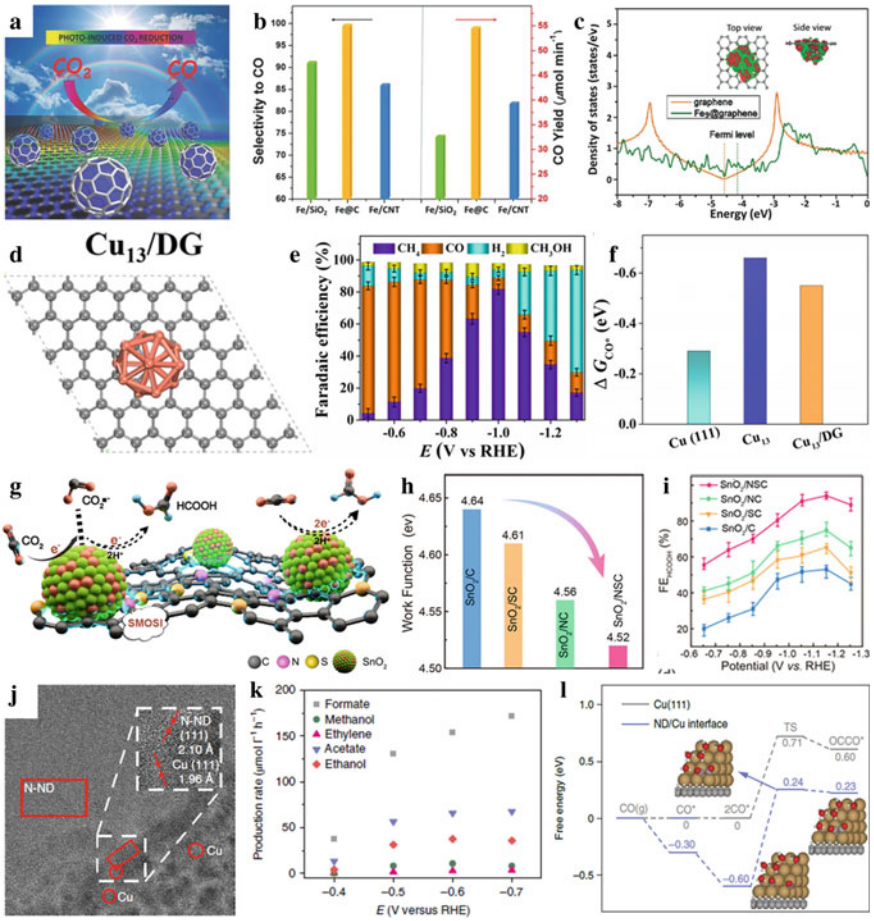

Fig. 8.4 Metal nanoparticles encapsulated and Metal nanoparticles supported carbon-based electrocatalysts. **a** Schematic illustration for the two-step preparation process for the core–shell structured Fe@C hybrid. **b** Photoinduced thermo-catalytic CO_2 conversion performance for Fe@C, Fe/SiO_2, and Fe/CNT catalysts in fixed bed reactor. **c** Projected density of states for the p_z orbitals of C atoms bonded with Fe atoms in the model of Fe_9@graphene in comparison with that of corresponding C atoms in pristine graphene model. The top and side views of the difference charge density of optimized Fe_9@graphene are shown as insertions. Reproduced with permission [62]. Copyright 2016, John Wiley and Sons. **d** Optimized structural model of Cu_{13}/DG. The pink and black represent Cu and C atoms, respectively. Faradaic efficiencies of **e** Cu/DRC at different potentials. **f** Adsorption energies of CO* intermediates on the above model. Reproduced with permission [63]. Copyright 2020, John Wiley and Sons. **g** Illustration of SMOSI enhancing the CO_2RR performance of SnO_2/NSC. **h** work function values. **i** FE_{HCOOH} and of SnO_2/C, SnO_2/SC, SnO_2/NC, and SnO_2/NSC. Reproduced with permission [26]. Copyright 2020, American Chemical Society. **j** HRTEM image of N-ND/Cu. The HRTEM image shows the presence of both Cu and nanodiamond as confirmed by lattice fringes of the selected regions in the micrograph. **k** Production rates for formate, methanol, ethylene, acetate and ethanol production by N-ND/Cu electrodes. **l** Free energy diagram for CO coupling on the Cu (111) surface (grey) and at the ND/Cu interface (blue). Reproduced with permission [64]. Copyright 2020, Springer Nature

electronic structure and improving the stability of the Cu clusters. Using molecular precursors, Hu et al. [26] have carefully designed a variety of doped and undoped carbon carriers with similar specific surface area, morphology and porous structure. It was found that these carriers were able to effectively load high density and small size SnO_2 NPs with a loading of approximately 60 wt.%. More importantly, systematic characterizations clearly revealed the existence of strong metal oxide-carrier interactions (SMOSI) between the SnO_2 nanoparticles and the doped carbon carriers (Fig. 8.4 g, h). The results show that the strongest SMOSI, SnO_2/NSC, has a CO_2RR selectivity of up to 94.4% for HCOOH and a partial current density of up to 56.0 mA cm^{-2}, which is superior to most Sn-based catalysts (Fig. 8.4i). Cui et al. [64] created a selective and reliable catalytic interface during the reduction of CO_2 to C_2 oxygenates by rationally tuning the assembly of N-doped nanodiamonds and copper nanoparticles (Fig. 8.4j). The catalyst exhibits a Faradaic efficiency of about 63% for C_2 oxygenates at an applied potential of only −0.5 V versus RHE (Fig. 8.4 k). In addition, the catalyst exhibits extremely high stability for up to 120 h. DFT calculations show that the binding of CO at the Cu/nanodiamond interface is significantly enhanced, reducing the apparent potential barrier of CO dimers and inhibiting the desorption of CO, thereby promoting the generation of C_2 (Fig. 8.4l). The design principles of this interface material-material platform will be applicable to various catalytic transformations, especially those requiring renewable energy input and aqueous conditions.

8.5 Conclusion and Perspectives

This chapter mainly introduces the research progress of carbon-based nanomaterials for CO_2 electrocatalytic reduction in recent years. Several efficient and typical carbon-based nanomaterials (non-metals, atomically dispersed metals, and metal nanoparticles) are selected for discussion. The differences of CO_2 electroreduction efficiency, product distribution and reduction process on various catalysts were analyzed. The special catalytic properties of these carbon-based nanomaterials and the mechanism behind them have improved the ideas for the development of efficient catalysts. Although the research on CO_2 electrocatalytic reduction has lasted for nearly half a century, the related work is almost limited to the scope of the laboratory, and it is still far from practical industrial application. In summary, it is believed that future research on electrocatalytic reduction of CO_2 needs to make breakthroughs in the following aspects.

(1) Development of catalysts suitable for the reduction of CO_2 to alcohol products. Compared with other products of CO_2 electroreduction, alcohol liquid products have advantages in storage and transportation, and alcohols have higher energy density, so they are more suitable as target products to store CO_2 and electrical energy in the form of chemical energy. However, in many research reports, the conversion rate and the generation rate of alcohol are not ideal.

It is difficult to significantly increase the efficiency of alcohols by using only pure copper-based catalytic electrodes. Atomically dispersed metals are worth trying as catalytic materials, which are expected to catalyze the efficient and rapid reduction of CO_2 to alcohols.

(2) Analysis of the mechanism of CO_2 reduction. Due to the lack of strong direct experimental observations to analyze the reaction mechanism (especially the aqueous reaction system), many mechanisms in the CO_2 reduction process are speculated by theoretical calculations. The theoretical calculations not only provide a reference for analyzing the reaction mechanism, but also provide a basis for the design of new catalysts. With the guidance of theoretical calculation results, researchers can purposefully synthesize new catalysts. However, for the same reduction process, there are also differences in the theoretical calculation results given by different researchers, and the proposed reaction processes are also different. However, for the same reduction process, there are also differences in the theoretical calculation results given by different researchers, and the proposed reaction processes are also different.

References

1. Y. Chen, Y. Zhang, G. Fan, L. Song, G. Jia, H. Huang, S. Ouyang, J. Ye, Z. Li, Z. Zou, Cooperative catalysis coupling photo-/photothermal effect to drive sabatier reaction with unprecedented conversion and selectivity. Joule **5**, 3235–3251 (2021). https://doi.org/10.1016/j.joule.2021.11.009
2. S. Ning, H. Xu, Y. Qi, L. Song, Q. Zhang, S. Ouyang, J. Ye, Microstructure induced thermodynamic and kinetic modulation to enhance CO_2 photothermal reduction: a case of atomic-scale dispersed Co-N species anchored Co@C hybrid. ACS Catal. **10**, 4726–4736 (2020). https://doi.org/10.1021/acscatal.9b04963
3. N. Li, J. Liu, J.J. Liu, L.Z. Dong, Z.F. Xin, Y.L. Teng, Y.Q. Lan, Adenine components in biomimetic metal-organic frameworks for efficient CO_2 photoconversion. Angew. Chem. Int. Ed. **58**, 5226–5231 (2019). https://doi.org/10.1002/anie.201814729
4. D.U. Nielsen, X.-M. Hu, K. Daasbjerg, T. Skrydstrup, Chemically and electrochemically catalysed conversion of CO_2 to CO with follow-up utilization to value-added chemicals. Nat. Catal. **2**, 95–95 (2018). https://doi.org/10.1038/s41929-018-0152-z
5. M.S. Frei, C. Mondelli, A. Cesarini, F. Krumeich, R. Hauert, J.A. Stewart, D. Curulla Ferré, J. Pérez-Ramírez, Role of zirconia in indium oxide-catalyzed CO_2 hydrogenation to methanol. ACS Catal. **10**, 1133–1145 (2019). https://doi.org/10.1021/acscatal.9b03305
6. D.D. Zhu, J.L. Liu, S.Z. Qiao, Recent advances in inorganic heterogeneous electrocatalysts for reduction of carbon dioxide. Adv. Mater. **28**, 3423–3452 (2016). https://doi.org/10.1002/adma.201504766
7. W. Zhang, Y. Hu, L. Ma, G. Zhu, Y. Wang, X. Xue, R. Chen, S. Yang, Z. Jin, Progress and perspective of electrocatalytic CO_2 reduction for renewable carbonaceous fuels and chemicals. Advanced Science **5**, 1700275 (2018). https://doi.org/10.1002/advs.201700275
8. T. Zheng, K. Jiang, H. Wang, Recent advances in electrochemical CO_2-to-CO conversion on heterogeneous catalysts. Adv. Mater. **30**, e1802066 (2018). https://doi.org/10.1002/adma.201802066
9. S. Verma, S. Lu, P.J.A. Kenis, Co-electrolysis of CO_2 and glycerol as a pathway to carbon chemicals with improved technoeconomics due to low electricity consumption. Nat. Energy **4**, 466–474 (2019). https://doi.org/10.1038/s41560-019-0374-6

10. M. Liu, M. Liu, X. Wang, S.M. Kozlov, Z. Cao, P. De Luna, H. Li, X. Qiu, K. Liu, J. Hu, C. Jia, P. Wang, H. Zhou, J. He, M. Zhong, X. Lan, Y. Zhou, Z. Wang, J. Li, A. Seifitokaldani, C.T. Dinh, H. Liang, C. Zou, D. Zhang, Y. Yang, T.-S. Chan, Y. Han, L. Cavallo, T.-K. Sham, B.-J. Hwang, E.H. Sargent, Quantum-dot-derived catalysts for CO_2 reduction reaction. Joule **3**, 1703–1718 (2019). https://doi.org/10.1016/j.joule.2019.05.010
11. T.-T. Zhuang, Z.-Q. Liang, A. Seifitokaldani, Y. Li, P. De Luna, T. Burdyny, F. Che, F. Meng, Y. Min, R. Quintero-Bermudez, C.T. Dinh, Y. Pang, M. Zhong, B. Zhang, J. Li, P.-N. Chen, X.-L. Zheng, H. Liang, W.-N. Ge, B.-J. Ye, D. Sinton, S.-H. Yu, E.H. Sargent, Steering post-C–C coupling selectivity enables high efficiency electroreduction of carbon dioxide to multi-carbon alcohols. Nat. Catal. **1**, 421–428 (2018). https://doi.org/10.1038/s41929-018-0084-7
12. Y. Hori, Electrochemical CO_2 reduction on metal electrodes. Mod. Aspects Electrochem. **42**, 89–189 (2008). https://doi.org/10.1007/978-0-387-49489-0_3
13. X. Wan, X. Liu, Y. Li, R. Yu, L. Zheng, W. Yan, H. Wang, M. Xu, J. Shui, Fe-N-C electrocatalyst with dense active sites and efficient mass transport for high-performance proton exchange membrane fuel cells. Nat. Catal. **2**, 259–268 (2019). https://doi.org/10.1038/s41929-019-0237-3
14. S. Wang, H. Jiang, L. Song, Recent progress in defective carbon-based oxygen electrode materials for rechargeable zinc-air batteries. Batteries Supercaps **2**, 509–523 (2019). https://doi.org/10.1002/batt.201900001
15. K. Gong, F. Du, Z. Xia, M. Durstock, L. Dai, Nitrogen-doped carbon nanotube arrays with high electrocatalytic activity for oxygen reduction. Science **323**, 760–764 (2009). https://doi.org/10.1126/science.1168049
16. I.S. Amiinu, X. Liu, Z. Pu, W. Li, Q. Li, J. Zhang, H. Tang, H. Zhang, S. Mu, From 3D ZIF nanocrystals to Co-N_x/C nanorod array electrocatalysts for ORR, OER, and Zn-air batteries. Adv. Func. Mater. **28**, 1704638 (2018). https://doi.org/10.1002/adfm.201704638
17. Y. Jia, J. Chen, X. Yao, Defect electrocatalytic mechanism: concept, topological structure and perspective. Mater. Chem. Front. **2**, 1250–1268 (2018). https://doi.org/10.1039/c8qm00070k
18. C. Xie, D. Yan, W. Chen, Y. Zou, R. Chen, S. Zang, Y. Wang, X. Yao, S. Wang, Insight into the design of defect electrocatalysts: from electronic structure to adsorption energy. Mater. Today **31**, 47–68 (2019). https://doi.org/10.1016/j.mattod.2019.05.021
19. H. Zhao, C. Sun, Z. Jin, D.-W. Wang, X. Yan, Z. Chen, G. Zhu, X. Yao, Carbon for the oxygen reduction reaction: a defect mechanism. J. Mater. Chem. A **3**, 11736–11739 (2015). https://doi.org/10.1039/c5ta02229k
20. S. Liu, H. Yang, X. Su, J. Ding, Q. Mao, Y. Huang, T. Zhang, B. Liu, Rational design of carbon-based metal-free catalysts for electrochemical carbon dioxide reduction: a review. J. Energy Chem. **36**, 95–105 (2019). https://doi.org/10.1016/j.jechem.2019.06.013
21. H. Yang, Q. Lin, C. Zhang, X. Yu, Z. Cheng, G. Li, Q. Hu, X. Ren, Q. Zhang, J. Liu, C. He, Carbon dioxide electroreduction on single-atom nickel decorated carbon membranes with industry compatible current densities. Nat. Commun. **11**, 593 (2020). https://doi.org/10.1038/s41467-020-14402-0
22. T.K. Todorova, M.W. Schreiber, M. Fontecave, Mechanistic understanding of CO_2 reduction reaction (CO_2RR) toward multicarbon products by heterogeneous Copper-based catalysts. ACS Catal. **10**, 1754–1768 (2019). https://doi.org/10.1021/acscatal.9b04746
23. B. Zhang, J. Zhang, J. Shi, D. Tan, L. Liu, F. Zhang, C. Lu, Z. Su, X. Tan, X. Cheng, B. Han, L. Zheng, J. Zhang, Manganese acting as a high-performance heterogeneous electrocatalyst in carbon dioxide reduction. Nat. Commun. **10**, 2980 (2019). https://doi.org/10.1038/s41467-019-10854-1
24. D. Deng, K.S. Novoselov, Q. Fu, N. Zheng, Z. Tian, X. Bao, Catalysis with two-dimensional materials and their heterostructures. Nat. Nanotechnol. **11**, 218–230 (2016). https://doi.org/10.1038/nnano.2015.340
25. D. Deng, L. Yu, X. Chen, G. Wang, L. Jin, X. Pan, J. Deng, G. Sun, X. Bao, Iron encapsulated within pod-like carbon nanotubes for oxygen reduction reaction. Angew. Chem. Int. Ed. **52**, 371–375 (2013). https://doi.org/10.1002/anie.201204958

26. L.-P. Yuan, W.-J. Jiang, X.-L. Liu, Y.-H. He, C. He, T. Tang, J. Zhang, J.-S. Hu, Molecularly engineered strong metal oxide-support interaction enables highly efficient and stable CO_2 electroreduction. ACS Catal. **10**, 13227–13235 (2020). https://doi.org/10.1021/acscatal.0c03831
27. Y. Jiang, L. Yang, T. Sun, J. Zhao, Z. Lyu, O. Zhuo, X. Wang, Q. Wu, J. Ma, Z. Hu, Significant contribution of intrinsic carbon defects to oxygen reduction activity. ACS Catal. **5**, 6707–6712 (2015). https://doi.org/10.1021/acscatal.5b01835
28. J. Zhu, Y. Huang, W. Mei, C. Zhao, C. Zhang, J. Zhang, I.S. Amiinu, S. Mu, Effects of intrinsic pentagon defects on electrochemical reactivity of carbon nanomaterials. Angew. Chem. Int. Ed. **58**, 3859–3864 (2019). https://doi.org/10.1002/anie.201813805
29. J. Wu, T. Sharifi, Y. Gao, T. Zhang, P.M. Ajayan, Emerging carbon-based heterogeneous catalysts for electrochemical reduction of carbon dioxide into value-added chemicals. Adv. Mater. **31**, e1804257 (2019). https://doi.org/10.1002/adma.201804257
30. M. Chen, S. Wang, H. Zhang, P. Zhang, Z. Tian, M. Lu, X. Xie, L. Huang, W. Huang, Intrinsic defects in biomass-derived carbons facilitate electroreduction of CO_2. Nano Res. **13**, 729–735 (2020). https://doi.org/10.1007/s12274-020-2683-2
31. Q. Wu, J. Gao, J. Feng, Q. Liu, Y. Zhou, S. Zhang, M. Nie, Y. Liu, J. Zhao, F. Liu, J. Zhong, Z. Kang, A CO_2 adsorption dominated carbon defect-based electrocatalyst for efficient carbon dioxide reduction. J. Mater. Chem. A **8**, 1205–1211 (2020). https://doi.org/10.1039/c9ta11473d
32. W. Wang, L. Shang, G. Chang, C. Yan, R. Shi, Y. Zhao, G.I.N. Waterhouse, D. Yang, T. Zhang, Intrinsic carbon-defect-driven electrocatalytic reduction of carbon dioxide. Adv. Mater. **31**, e1808276 (2019). https://doi.org/10.1002/adma.201808276
33. S. Liu, H. Yang, X. Huang, L. Liu, W. Cai, J. Gao, X. Li, T. Zhang, Y. Huang, B. Liu, Identifying active sites of nitrogen-doped carbon materials for the CO_2 reduction reaction. Adv. Func. Mater. **28**, 1800499 (2018). https://doi.org/10.1002/adfm.201800499
34. L. Li, Y. Huang, Y. Li, Carbonaceous materials for electrochemical CO_2 reduction. EnergyChem **2**, 100024 (2020). https://doi.org/10.1016/j.enchem.2019.100024
35. J. Zhao, H. Lai, Z. Lyu, Y. Jiang, K. Xie, X. Wang, Q. Wu, L. Yang, Z. Jin, Y. Ma, J. Liu, Z. Hu, Hydrophilic hierarchical nitrogen-doped carbon nanocages for ultrahigh supercapacitive performance. Adv. Mater. **27**, 3541–3545 (2015). https://doi.org/10.1002/adma.201500945
36. M. Tomisaki, S. Kasahara, K. Natsui, N. Ikemiya, Y. Einaga, Switchable product selectivity in the electrochemical reduction of carbon dioxide using boron-doped diamond electrodes. J. Am. Chem. Soc. **141**, 7414–7420 (2019). https://doi.org/10.1021/jacs.9b01773
37. X. Zou, M. Liu, J. Wu, P.M. Ajayan, J. Li, B. Liu, B.I. Yakobson, How nitrogen-doped graphene quantum dots catalyze electroreduction of CO_2 to hydrocarbons and oxygenates. ACS Catal. **7**, 6245–6250 (2017). https://doi.org/10.1021/acscatal.7b01839
38. Z. Ma, L. Tao, D. Liu, Z. Li, Y. Zhang, Z. Liu, H. Liu, R. Chen, J. Huo, S. Wang, Ultrafine nano-sulfur particles anchored on in situ exfoliated graphene for lithium–sulfur batteries. J. Mater. Chem. A **5**, 9412–9417 (2017). https://doi.org/10.1039/c7ta01981e
39. J. Kim, R. Zhou, K. Murakoshi, S. Yasuda, Advantage of semi-ionic bonding in fluorine-doped carbon materials for the oxygen evolution reaction in alkaline media. RSC Adv. **8**, 14152–14156 (2018). https://doi.org/10.1039/c8ra01636d
40. T. Liu, S. Ali, Z. Lian, C. Si, D.S. Su, B. Li, Phosphorus-doped onion-like carbon for CO_2 electrochemical reduction: the decisive role of the bonding configuration of phosphorus. J. Mater. Chem. A **6**, 19998–20004 (2018). https://doi.org/10.1039/c8ta06649c
41. W. Li, M. Seredych, E. Rodriguez-Castellon, T.J. Bandosz, Metal-free nanoporous carbon as a catalyst for electrochemical reduction of CO_2 to CO and CH_4. Chemsuschem **9**, 606–616 (2016). https://doi.org/10.1002/cssc.201501575
42. P. Wu, Y. Qian, P. Du, H. Zhang, C. Cai, Facile synthesis of nitrogen-doped graphene for measuring the releasing process of hydrogen peroxide from living cells. J. Mater. Chem. **22**, 6402–6412 (2012). https://doi.org/10.1039/c2jm16929k
43. X. Cui, Z. Pan, L. Zhang, H. Peng, G. Zheng, Selective etching of nitrogen-doped carbon by steam for enhanced electrochemical CO_2 reduction. Adv. Energy Mater. **7**, 1701456 (2017). https://doi.org/10.1002/aenm.201701456

44. W. Feng, P. Long, Y. Feng, Y. Li, Two-dimensional fluorinated graphene: synthesis, structures, properties and applications. Adv. Sci. **3**, 1500413 (2016). https://doi.org/10.1002/advs.201500413
45. J. Xie, X. Zhao, M. Wu, Q. Li, Y. Wang, J. Yao, Metal-free fluorine-doped carbon electrocatalyst for CO_2 reduction outcompeting hydrogen evolution. Angew. Chem. Int. Ed. **57**, 9640–9644 (2018). https://doi.org/10.1002/anie.201802055
46. X. Xue, H. Yang, T. Yang, P. Yuan, Q. Li, S. Mu, X. Zheng, L. Chi, J. Zhu, Y. Li, J. Zhang, Q. Xu, N, P-coordinated fullerene-like carbon nanostructures with dual active centers toward highly-efficient multi-functional electrocatalysis for CO2RR ORR and Zn-air battery. J. Mater. Chem. A **7**, 15271–15277 (2019). https://doi.org/10.1039/c9ta03828k
47. Z. Wang, H. Jin, T. Meng, K. Liao, W. Meng, J. Yang, D. He, Y. Xiong, S. Mu, Fe, Cu-coordinated ZIF-derived carbon framework for efficient oxygen reduction reaction and zinc-air batteries. Adv. Func. Mater. **28**, 1802596 (2018). https://doi.org/10.1002/adfm.201802596
48. T. Ouyang, Y.Q. Ye, C.Y. Wu, K. Xiao, Z.Q. Liu, Heterostructures composed of N-doped carbon nanotubes encapsulating cobalt and beta-Mo_2C nanoparticles as bifunctional electrodes for water splitting. Angew. Chem. Int. Ed. **58**, 4923–4928 (2019). https://doi.org/10.1002/anie.201814262
49. C. Hu, R. Paul, Q. Dai, L. Dai, Carbon-based metal-free electrocatalysts: from oxygen reduction to multifunctional electrocatalysis. Chem. Soc. Rev. **50**, 11785–11843 (2021). https://doi.org/10.1039/d1cs00219h
50. J.N. Kuhn, W. Huang, C.K. Tsung, Y. Zhang, G.A. Somorjai, Structure sensitivity of carbon-nitrogen ring opening: Impact of platinum particle size from below 1 to 5 nm upon pyrrole hydrogenation product selectivity over monodisperse platinum nanoparticles loaded onto mesoporous silica. J. Am. Chem. Soc. **130**, 14026–14027 (2008). https://doi.org/10.1021/ja805050c
51. Y. Wang, P. Han, X. Lv, L. Zhang, G. Zheng, Defect and interface engineering for aqueous electrocatalytic CO_2 reduction. Joule **2**, 2551–2582 (2018). https://doi.org/10.1016/j.joule.2018.09.021
52. A.S. Varela, N. Ranjbar Sahraie, J. Steinberg, W. Ju, H.S. Oh, P. Strasser, Metal-doped nitrogenated carbon as an efficient catalyst for direct CO_2 electroreduction to CO and hydrocarbons. Angew. Chem. Int. Ed. **54**, 10758–10762 (2015). https://doi.org/10.1002/anie.201502099
53. Q. He, J.H. Lee, D. Liu, Y. Liu, Z. Lin, Z. Xie, S. Hwang, S. Kattel, L. Song, J.G. Chen, Accelerating CO_2 electroreduction to CO over Pd single-atom catalyst. Adv. Func. Mater. **30**, 2000407 (2020). https://doi.org/10.1002/adfm.202000407
54. X. Sun, Y. Tuo, C. Ye, C. Chen, Q. Lu, G. Li, P. Jiang, S. Chen, P. Zhu, M. Ma, J. Zhang, J.H. Bitter, D. Wang, Y. Li, Phosphorus induced electron localization of single iron sites for boosted CO_2 electroreduction reaction. Angew. Chem. Int. Ed. **60**, 23614–23618 (2021). https://doi.org/10.1002/anie.202110433
55. K.P. Kuhl, T. Hatsukade, E.R. Cave, D.N. Abram, J. Kibsgaard, T.F. Jaramillo, (2014) Electrocatalytic conversion of carbon dioxide to methane and methanol on transition metal surfaces. Journal of the American Chemical Society, 136: 14107–14113. https://doi.org/10.1021/ja505791r
56. A. Vasileff, C. Xu, Y. Jiao, Y. Zheng, S.-Z. Qiao, Surface and interface engineering in copper-based bimetallic materials for selective CO_2 electroreduction. Chem **4**, 1809–1831 (2018). https://doi.org/10.1016/j.chempr.2018.05.001
57. H. Yang, Y. Wu, G. Li, Q. Lin, Q. Hu, Q. Zhang, J. Liu, C. He, Scalable production of efficient single-atom copper decorated carbon membranes for CO_2 electroreduction to methanol. J. Am. Chem. Soc. **141**, 12717–12723. https://doi.org/10.1021/jacs.9b04907
58. E. Zhang, T. Wang, K. Yu, J. Liu, W. Chen, A. Li, H. Rong, R. Lin, S. Ji, X. Zheng, Y. Wang, L. Zheng, C. Chen, D. Wang, J. Zhang, Y. Li, Bismuth single atoms resulting from transformation of metal-organic frameworks and their use as electrocatalysts for CO_2 reduction. J. Am. Chem. Soc. **141**, 16569–16573 (2019). https://doi.org/10.1021/jacs.9b08259
59. P. Song, M. Luo, X. Liu, W. Xing, W. Xu, Z. Jiang, L. Gu, Zn single atom catalyst for highly efficient oxygen reduction reaction. Adv. Func. Mater. **27**, 1700802 (2017). https://doi.org/10.1002/adfm.201700802

60. W. Zhu, L. Zhang, S. Liu, A. Li, X. Yuan, C. Hu, G. Zhang, W. Deng, K. Zang, J. Luo, Y. Zhu, M. Gu, Z.J. Zhao, J. Gong, Enhanced CO_2 electroreduction on neighboring Zn/Co monomers by electronic effect. Angew. Chem. Int. Ed. **59**, 12664–12668 (2020). https://doi.org/10.1002/anie.201916218
61. T. Zhang, X. Han, H. Liu, M. Biset-Peiró, X. Zhang, P. Tan, P. Tang, B. Yang, L. Zheng, J.R. Morante, J. Arbiol, Quasi-double-star nickel and iron active sites for high-efficiency carbon dioxide electroreduction. Energy Environ. Sci. **14**, 4847–4857 (2021). https://doi.org/10.1039/d1ee01592c
62. H. Zhang, T. Wang, J. Wang, H. Liu, T.D. Dao, M. Li, G. Liu, X. Meng, K. Chang, L. Shi, T. Nagao, J. Ye, Surface-plasmon-enhanced photodriven CO_2 reduction catalyzed by metal-organic-framework-derived iron nanoparticles encapsulated by ultrathin carbon layers. Adv. Mater. **28**, 3703–3710 (2016). https://doi.org/10.1002/adma.201505187
63. Q. Hu, Z. Han, X. Wang, G. Li, Z. Wang, X. Huang, H. Yang, X. Ren, Q. Zhang, J. Liu, C. He, Facile synthesis of sub-nanometric copper clusters by double confinement enables selective reduction of carbon dioxide to methane. Angew. Chem. Int. Ed. **59**, 19054–19059 (2020). https://doi.org/10.1002/anie.202009277
64. H. Wang, Y.K. Tzeng, Y. Ji, Y. Li, J. Li, X. Zheng, A. Yang, Y. Liu, Y. Gong, L. Cai, Y. Li, X. Zhang, W. Chen, B. Liu, H. Lu, N.A. Melosh, Z.X. Shen, K. Chan, T. Tan, S. Chu, Y. Cui, Synergistic enhancement of electrocatalytic CO_2 reduction to C_2 oxygenates at nitrogen-doped nanodiamonds/Cu interface. Nat. Nanotechnol. **15**, 131–137 (2020). https://doi.org/10.1038/s41565-019-0603-y